

Three-dimensional whole-head optical tomography of passive motor evoked responses in the neonate

A.P. Gibson,^{a,*} T. Austin,^b N.L. Everdell,^a M. Schweiger,^c S.R. Arridge,^c J.H. Meek,^b
J.S. Wyatt,^b D.T. Delpy,^a and J.C. Hebden^a

^aDepartment of Medical Physics and Bioengineering, University College London, Malet Place Engineering Building, London WC1E 6BT, UK

^bDepartment of Paediatrics and Child Health, University College London, 5 University Street, London WC1E 6JJ, UK

^cDepartment of Computer Science, University College London, Malet Place Engineering Building, London WC1E 6BT, UK

Received 13 April 2005; revised 8 July 2005; accepted 30 August 2005
Available online 24 October 2005

Optical tomography has been used to reconstruct three-dimensional images of the entire neonatal head during motor evoked responses. Data were successfully acquired during passive movement of each arm on four out of six infants examined, from which eight sets of bilateral images of hemodynamic parameters were reconstructed. Six out of the eight images showed the largest change in total hemoglobin in the region of the contralateral motor cortex. The mean distance between the peak response in the image and the estimated position of the contralateral motor cortex was 10.8 mm. These results suggest that optical tomography may provide an appropriate technique for non-invasive cot-side imaging of brain function.

© 2005 Elsevier Inc. All rights reserved.

Introduction

Optical tomography is a medical imaging technique in which measurements of near-infrared light transmitted across the body are used to obtain images of the optical properties of tissue (Boas et al., 2001a, Schweiger et al., 2003, Gibson et al., 2005a). Unlike the popular technique of optical *topography*, which produces 2D images of activated regions on the surface of the brain (Strangman et al., 2002, Hebden, 2003, Koizumi et al., 2003), optical *tomography* produces 3D volumetric images of the whole head and hence can identify changes occurring in deeper tissues. Certain components of tissue have optical properties which are wavelength-dependent, such as the absorption spectra of oxy- and deoxyhemoglobin. Optical tomography using multiple wavelengths therefore allows images of the concentration of oxy- and deoxyhemoglobin ([HbO₂], [HHb]) to be generated. Furthermore, an optical imaging system is portable and can be used for safe, continuous monitoring at the bedside.

Both preterm and term infants are vulnerable to cerebral injury in the perinatal period, and such damage can occur deep within the brain (Volpe, 2001). The principal motivation for our work has been to assess regional cerebral blood volume and oxygenation in the newborn, both to improve our understanding of the pathophysiology of perinatal brain injury and to identify vulnerable infants who may benefit from new neuroprotective therapies (Hebden, 2003, Gluckmann et al., 2005). Optical images of the infant cortex have previously been obtained using optical topography (e.g., Taga et al. (2003), Tsujimoto et al. (2004)), and the adult brain has been imaged by limited volume tomography (Bluestone et al., 2001). However, these techniques provide little information about deeper regions of the brain. We have, therefore, concentrated on reconstructing the full 3D volume by measuring light which has been transmitted across the whole head. The first work of this nature (Hintz et al., 1999) required scan times of several hours and used a relatively crude reconstruction technique to provide 2D images which did, nevertheless, correlate with those from other imaging methods. More recently, we have generated the first 3D optical images of an intraventricular hemorrhage in the neonatal brain which correlated with ultrasound images (Hebden et al., 2002). We have also produced functional images during swings in blood oxygen and carbon dioxide concentration caused by modifying the ventilator settings of a severely brain-injured infant (Hebden et al., 2004). These images agreed with the expected physiological changes.

While we have validated images obtained in the laboratory on tissue-equivalent phantoms (Gibson et al., 2003b), clinical validation is necessary before the technique can be widely accepted. However, as optical tomography is the only method which can produce images of brain function at the cot-side, there is no “gold standard” imaging technique against which it can be compared. An alternative method by which optical tomography can be validated is to image a known functional change and correlate its localization with known anatomy. In this paper, we present 3D optical tomography images obtained during passive motor evoked

* Corresponding author. Fax: +44 20 7679 0255.

E-mail address: agibson@medphys.ucl.ac.uk (A.P. Gibson).

Available online on ScienceDirect (www.sciencedirect.com).

responses induced by raising and lowering an infant's arm and show that the reconstructed change in optical properties agrees with the expected anatomical position of the contralateral motor cortex.

Method

Instrumentation

To detect light which has been transmitted across the entire head within a timescale which is clinically acceptable, a powerful light source and sensitive photon-counting detectors are required. With this in mind, we have built a system called MONSTIR (multi-channel opto-electronic system for time-resolved image reconstruction) which has a fiber laser source and 32 parallel time-resolved single-photon counting detectors (Schmidt et al., 2000). A dual fiber laser (IMRA Inc., USA) provides light pulses of 2-ps duration at 780 nm and 815 nm which are coupled sequentially via an optical fiber switch into one of 32 connectors on the head. Each fiber consists of a co-axial source fiber surrounded by a detector fiber bundle, and terminates in a connector (an "optode") which holds the source and detector 10 mm from the scalp. This ensures even illumination, increases the detection area, reduces the effect of hair beneath the connectors and allows calibration by measurement of back-reflected light (Hebden et al., 2003). Light from the active source is collected simultaneously by all the other detectors and coupled into four 8-anode microchannel plate photomultiplier tubes in photon-counting mode. The dynamic range of the detected light is reduced by a set of variable optical attenuators, to minimize the number of detectors which saturate. The arrival times of detected photons are compared to a reference signal from the laser and histograms of photon flight times, or temporal point spread functions (TPSFs) are accumulated. A full set of data consists of 31 measurements from each of 32 sources, although in practice, measurements with small source–detector separations would saturate the detectors and are rejected, giving typically 800 TPSFs per image data set. The 32 optodes are held in a semi-rigid thermoplastic helmet which is lined with infrared absorbing foam so that the optodes are optically isolated from each other. Currently, a new helmet is custom-built for each infant (Fig. 1). Light from



Fig. 1. Activating the right arm of a neonate wearing a helmet with optical tomography connectors.

the laser is attenuated to ensure the power is less than 15 mW, which is eyesafe according to the British safety standards (Amendment 2 (2001) to BS EN 60825-1, "Safety of laser products").

Image reconstruction

Near-infrared light travels through tissue predominantly by scatter, so much of the spatial information in the measured signal is lost (a typical mean photon flight time is almost an order of magnitude greater than the time required for the most direct path). The image reconstruction problem is consequently ill posed—a change in optical properties may lead to an arbitrarily large change in the measurements. The solution is highly sensitive to the geometry of the problem, the positions and coupling of the sources and detectors, and errors in the data or the image reconstruction. To reduce these effects, rather than reconstructing images of the absolute optical properties during activation, images were obtained of the difference in the optical properties during activation compared to a resting state. Evoked responses provide a close to ideal situation for this type of imaging as the resting state can be assumed to be identical to the activation state with the exception of a single spatially localized perturbation. We have recently shown that where reference data are available which closely match data acquired following a change, linear reconstruction may provide superior image quality compared to non-linear (Gibson et al., 2005b).

The diffusion of light across the head was modeled using the finite element method (Arridge et al., 2000). This requires a finite element mesh upon whose surface the optodes lie and which conforms to the shape of the head. The surface of the finite element mesh was generated by warping a known head-like surface so that it passed through the positions of the optodes (Gibson et al., 2003a) which were measured using a 3D digitizing arm (Microscribe 3D, Immersion Co., USA). A finite element mesh was generated from this surface using Netgen (Schöberl, 1997). The mesh parameters were different for each infant but typically included 20,000 elements with quadratic interpolation functions. Minimizing the mesh density was not seen as a priority as the Jacobian is pre-computed in linear reconstruction.

The information content of the TPSFs was compressed by Fourier transforming them and extracting the amplitude A and phase ϕ at a given frequency (100 MHz was used in this work). This reduces the amount of data which the reconstruction algorithm has to process and considerably speeds up the image reconstruction. Prior to image reconstruction, the problem was linearized by the Rytov approximation (Arridge, 1999) such that changes in A and ϕ were related to changes in the absorption coefficient μ_a and diffusion coefficient $\kappa = 1/3(\mu_a + \mu'_s)$, where μ'_s is the transport scattering coefficient, by the matrix equation

$$\Delta \begin{pmatrix} A \\ \phi \end{pmatrix} = \begin{pmatrix} \mathbf{J}_{\mu_a}^A & \mathbf{J}_{\kappa}^A \\ \mathbf{J}_{\mu_a}^{\phi} & \mathbf{J}_{\kappa}^{\phi} \end{pmatrix} \Delta \begin{pmatrix} \mu_a \\ \kappa \end{pmatrix}, \quad (1)$$

where \mathbf{J}_x^y is the Jacobian of the forward mapping for the change in data type $\Delta y = \Delta \begin{pmatrix} A \\ \phi \end{pmatrix}$ and change in optical parameter $\Delta x = \Delta \begin{pmatrix} \mu_a \\ \kappa \end{pmatrix}$. The Jacobian matrix $\mathbf{J} = \begin{pmatrix} \mathbf{J}_{\mu_a}^A & \mathbf{J}_{\kappa}^A \\ \mathbf{J}_{\mu_a}^{\phi} & \mathbf{J}_{\kappa}^{\phi} \end{pmatrix}$ was found by solving the diffusion equation with the finite element method, using the forward and adjoint solutions to construct sensitivity functions (Arridge and Schweiger, 1995).

Complications arise because Δy consists of measurements of both log amplitude and phase, and Δx includes images of both absorption coefficient μ_a and reduced scatter coefficient μ'_s . These issues were addressed by normalizing \mathbf{J} , Δy and Δx as follows:

(1) Δx and \mathbf{J} were normalized by dividing by the mean optical parameters to ensure that μ_a and μ'_s contribute equally to the image reconstruction. We define a matrix $\mathbf{S} = \begin{pmatrix} \bar{\mu}_a & 0 \\ 0 & \bar{\kappa} \end{pmatrix}$ and a scaled data vector $\tilde{x} = \mathbf{S}^{-1}x$ such that Eq. (1) becomes

$$\Delta y = \mathbf{J} \mathbf{S} \Delta \tilde{x}. \quad (2)$$

(2) The magnitude, dimension and error of the log amplitude and phase data types are different. This was corrected by dividing both by their respective standard deviations. If $\sigma = \begin{pmatrix} \sigma^A \\ \sigma^\phi \end{pmatrix}$, where σ^x is the standard deviation of data type x , then Eq. (2) becomes

$$\left(\frac{\Delta y}{\sigma} \right) = \frac{1}{\sigma} \mathbf{J} \mathbf{S} \Delta \tilde{x}. \quad (3)$$

(3) The image reconstruction is regularized according to the L_2 -norm of the data. This is different for the log amplitude and the phase, implying that each has a different influence on the image reconstruction. This could be dealt with by applying different regularization parameters for A and ϕ , but instead, the data were normalized to the sum of the squares of the data, i.e., we define

$$\mathbf{C} \begin{pmatrix} \text{diag}(C_1) & 0 \\ 0 & \text{diag}(C_2) \end{pmatrix}^{-1}, \text{ where } C_{1i} = \sum \left(\frac{\Delta A}{\sigma^A} \right)^2 \text{ and } C_{2i} = \sum \left(\frac{\Delta \phi}{\sigma^\phi} \right)^2,$$

for $i = 1 \dots n$ where n is the number of measurements, and apply this to Eq. (3):

$$\mathbf{C} = \left(\frac{\Delta y}{\sigma} \right) = \frac{\mathbf{C}}{\sigma} \mathbf{J} \mathbf{S} \Delta \tilde{x}. \quad (4)$$

Eq. (4) was inverted following Tikhonov regularization of the Moore–Penrose generalized inverse $\Delta \tilde{x} = \tilde{\mathbf{J}}(\tilde{\mathbf{J}}\tilde{\mathbf{J}}^T + \lambda \mathbf{I})\mathbf{C}(\Delta y/\sigma)$, where T denotes the matrix transpose, \mathbf{I} is the identity matrix and $\tilde{\mathbf{J}} = (\mathbf{C}/\sigma)\mathbf{J}\mathbf{S}$.

(4) The effect of coupling between the optode and the tissue was included in the reconstruction using the augmented Jacobian method described by Boas et al. (2001b).

Regularization was performed by adjusting the parameter λ which, in this work, was set at 10% of the maximum singular value of $\mathbf{J}\tilde{\mathbf{J}}^T$. After examining a range of λ from 0.01% to 100%, 10% appeared to give smooth, relatively artefact-free images which were quantitatively plausible. This corresponds to a mismatch between data and the model of 10% which is larger than the measured experimental error of about 1% but includes the error due to the mismatch between the homogeneous model and the data collected on the neonatal head. The rescaling of \mathbf{J} , Δy and Δx affects the optimal λ in a complicated manner.

Separate images of μ_a and μ'_s were reconstructed at 780 and 815 nm. The absorption images were combined using the Beer–Lambert Law as described by Hueber et al. (2001) to provide images of $\Delta[\text{HHb}]$ and $\Delta[\text{HbO}_2]$ which were summed to provide images of $\Delta[\text{HbT}]$.

Experimental method

Evoked response studies were performed on six very preterm infants at about 1 month of age (Table 1). The infants were selected for study because they were of appropriate head circumference and clinically stable. The median (range) postmenstrual age at birth was 28 weeks 5 days (28w 2d to 32w 1d), and the median (range) corrected age when imaged was 34 weeks 5 days (33w 6d to 36w 5d). Two pairs of the babies were twins. Two of the babies had intraventricular hemorrhages at birth, one of which had resolved by the time of the study leaving a dilated ventricle. Ethical permission for the study was obtained from the local ethics committee, and informed consent was obtained from the parents prior to the study.

A helmet was custom-built for each baby which could hold up to 32 optodes. For the smallest babies, there was only room on the head to support 28 optodes while maintaining adequate optical isolation between each (Fig. 1).

To detect light which has been transmitted across the whole head with adequate signal-to-noise ratio, it was necessary to sum the signal from each source for 10 s. Light is detected on all channels in parallel, so a single image takes about 11 min to acquire (10 s \times 32 sources, plus data download and switching time between sources). This is too long for imaging evoked responses which reduce in amplitude due to habituation after about 30 s even if the activation task is maintained. For this study, the effective

Table 1
Summary of images obtained from the 6 babies examined

	Corrected age at study	Cranial ultrasound appearance	Data obtained?	Distance from peak [HbT] to contralateral motor cortex	Peak $\Delta[\text{HbT}]$ (μM)
Baby 1	33 weeks, 6 days	Bilateral intraventricular hemorrhage	NO	–	–
Baby 2	33 weeks, 5 days	Normal	YES	L 5 mm R No localized change	26 –
Baby 3	36 weeks, 5 days	Normal	YES	L 18 mm R 14.8 mm	15
Baby 4	36 weeks, 5 days	Normal	NO	–	–
Baby 5	34 weeks, 5 days	Normal	YES	L 10.8 mm R 5.2 mm	10 36
Baby 6	34 weeks, 5 days	Left intraventricular hemorrhage	YES	L No localized change R 11.5 mm Mean 10.8 mm	– 25 25

Babies 3 and 4, and babies 5 and 6, are twins. Images acquired during left passive motor activation on babies 2 and 3 are shown in Figs. 4 and 5, respectively.

acquisition time was reduced to 10 s by activating a single source and recording resting baseline activity for 10 s, then inducing activation by passive movement of an arm for 15 s, with activation data acquired using the same source during the last 10 s (Fig. 2). This was repeated for up to 12 different sources; after this, the baby tended to become restless. In practice, this provided about 320 measurements (source–detector pairs) per image.

The activation exercise involved passively raising and lowering the left or right arm. This activation can be performed on a sleeping baby, stimulating activity which is spatially localized to the sensory and motor cortices, and providing good spatial separation between left and right cortical activity. In total, a full experiment involving 12 sources with bilateral activation including calibration measurements took about 2 h, so it could be conducted between feeding times when the baby was most passive.

Results

Data quality

Data were successfully acquired from four of the six infants examined (see Table 1). The two infants on whom data were not successfully acquired were the first infant we examined, when the experimental procedure was still being developed, and a later study which was affected by movement artefact. Both these studies were abandoned, and images were not reconstructed.

Light leaking from a source around the head to a detector due to insufficient contact between the head and the helmet was a recurring problem. Babies were positioned with their head raised to minimize the effect of gastro-esophageal reflux. This reduces irritation and therefore movement but increases the likelihood that the baby will slip out of the helmet. Fig. 3 shows temporal point spread functions (TPSFs) acquired for a single source–detector combination during activation (top) and at rest (bottom). The TPSFs are smooth and contain about 400,000 photons. The TPSF acquired during activation can be seen to be preceded by a “pre-peak” (Hillman et al., 2000). This is due to light leaking between optodes through air and therefore arriving before the diffuse light which has passed through the head. Such a pre-peak has a greater effect on the amplitude and mean photon flight time than that of the activation and will therefore lead to artefacts in the image. Examination of the time-domain data allows erroneous TPSFs such as these to be identified and eliminated from the image reconstruction. The remaining data types were then examined further by plotting them against optode separation, and any outliers, determined by their deviation from an approximate straight line fit, were excluded. Typically between 30 and 60 measurements were rejected out of a total of 320, usually because

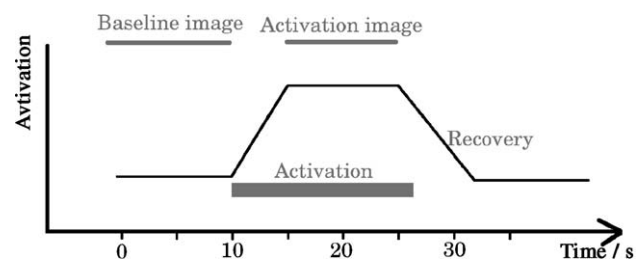


Fig. 2. Schematic illustration of the activation paradigm. The horizontal grey bar shows the period of activation.

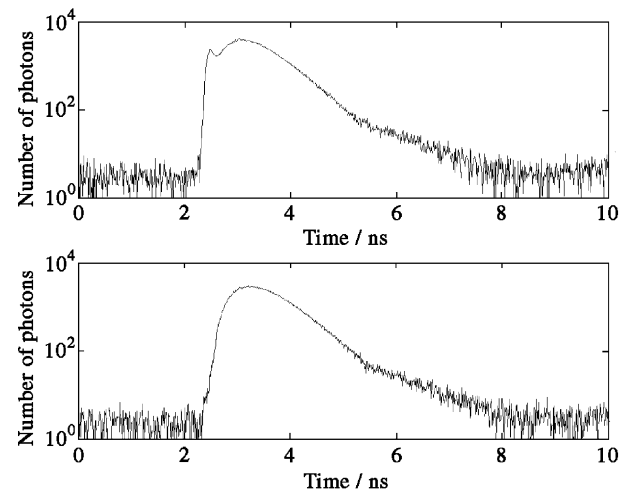


Fig. 3. Temporal point spread functions acquired on an infant. The top image shows data acquired during stimulation, the bottom image is the corresponding reference data. The pre-peak visible on the top image is due to light escaping from the head and will overwhelm any changes in the TPSF due to the stimulation. Effects such as these can be eliminated by examination of time-domain data.

of light leakage or intermittent instability in one of the detector channels.

Images of absorption and scatter

Images of bilateral evoked responses were successfully reconstructed from the remaining four infants. Six of the eight sets of images showed an increase in optical absorption in the region of the contralateral motor cortex at both wavelengths. The mean (\pm standard deviation) increase in absorption in the 6 successfully reconstructed images was $(0.0129 \pm 0.0016) \text{ mm}^{-1}$ at 780 nm and $(0.0123 \pm 0.0011) \text{ mm}^{-1}$ at 815 nm. This represents a localized increase in absorption of approximately 29% at 780 nm at which deoxyhemoglobin absorbs most strongly, and 23% at 815 nm where oxyhemoglobin is the strongest absorber. By comparison, the maximum change in scatter was 5% (the mean was 2%). The scatter images showed little physiological change and consisted primarily of measurement noise and cross-talk from the larger change in absorption.

Images of functional change

The reconstructed images of absorption at 780 and 815 nm were converted into images of absolute change in oxy- and deoxy- and total hemoglobin ($\Delta[\text{HbO}_2]$, $\Delta[\text{HHb}]$ and $\Delta[\text{HbT}]$, respectively) as described in Section 2.2. The position of the representation of the arm in the motor cortex was estimated from knowledge of the anatomy of the neonatal brain and, in the six out of eight examples which demonstrated correctly localized images of absorption, the peak $\Delta[\text{HbT}]$ was in the region of the contralateral motor cortex. The mean distance from the peak change in $[\text{HbT}]$ to the estimated position of the motor cortex was 10.8 mm (see Table 1). Fig. 4 shows a series of sagittal slices of $\Delta[\text{HbT}]$ obtained during activation of the left arm. The peak change in the image occurs 18.0 mm from the estimated position of the right motor cortex (denoted by a cross), which was the largest error observed. Fig. 5 shows similar images of $\Delta[\text{HbO}_2]$, $\Delta[\text{HHb}]$ and $\Delta[\text{HbT}]$ in a different individual.

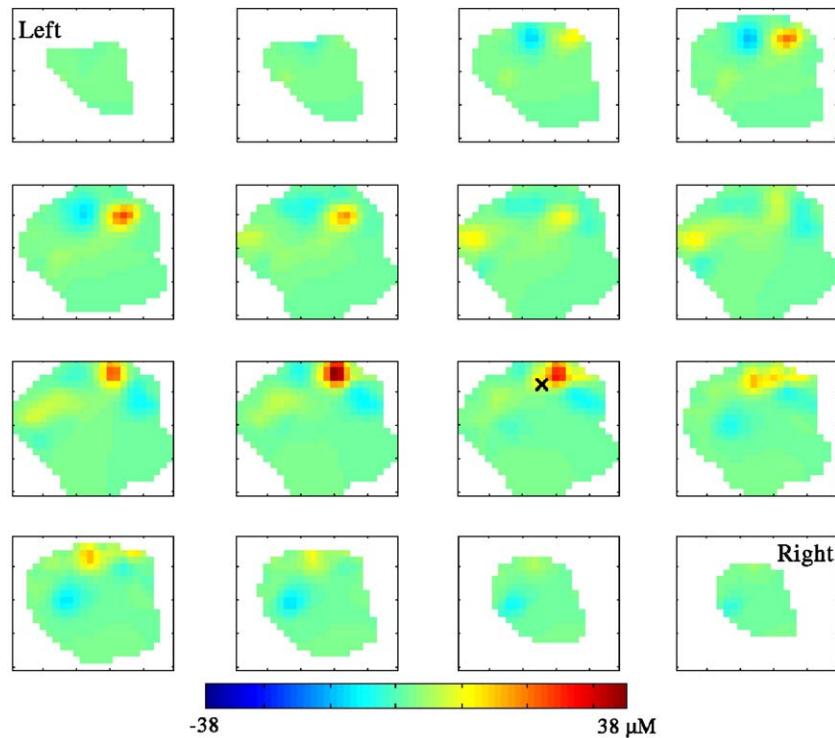


Fig. 4. Image of $\Delta[\text{HbT}]$ during left motor activity, showing an increase near the estimated position of the motor cortex (denoted by a cross). This figure shows 16 sagittal slices from the left (top right) to the right (bottom left) of the head. Each voxel corresponds to approximately 5 mm^3 .

In four out of the six images in which $\Delta[\text{HbT}]$ was localized to the estimated position of the contralateral motor cortex, the peak change in $\Delta[\text{HHb}]$ and $\Delta[\text{HbO}_2]$ also coincided with the motor cortex. To estimate the change in the hemodynamic parameters in the contralateral motor cortex, a region was defined with a radius 25 mm around its estimated position and the peak increase and peak decrease in $[\text{HHb}]$, $[\text{HbO}_2]$ and $[\text{HbT}]$ found in this region for each of the 6 successfully localized images. The mean (\pm standard deviation) peak increases in $[\text{HbO}_2]$, $[\text{HHb}]$ and $[\text{HbT}]$ were $25 \pm 17 \mu\text{M}$, $27 \pm 20 \mu\text{M}$ and $25 \pm 11 \mu\text{M}$, respectively. These values are substantially higher than the mean peak decreases in $[\text{HbO}_2]$, $[\text{HHb}]$ and $[\text{HbT}]$ which were $19 \pm 12 \mu\text{M}$, $16 \pm 14 \mu\text{M}$ and $6 \pm 5 \mu\text{M}$, respectively. This suggests that the predominant change in the contralateral motor cortex was an increase in both $[\text{HHb}]$ and $[\text{HbO}_2]$, leading to an overall increase in $[\text{HbT}]$. In four out of the six images which showed correct localization, the increase in $[\text{HHb}]$ was greater than the increase in $[\text{HbO}_2]$.

Discussion

Localization accuracy

In six out of eight sets of images, absorption increased in the region of the contralateral motor cortex, suggesting an increase in blood volume. This was confirmed by the predominant increase in $[\text{HbT}]$ which occurred a mean distance of 10.8 mm from the estimated position of the motor cortex.

A significant contribution to the localization error comes from warping the head-shaped surface to fit the measured positions of the optodes to create the finite element mesh. The warp is carried out with no control points in common between the surface and the

connectors. The connectors are aligned with the surface by eye, and although the resulting surface is sufficiently accurate for use in difference imaging (Gibson et al., 2003a), any misalignment will contribute to localization errors. The positions of the optodes are visually realigned by typically 5 mm in the y -axis and z -axis (the x -axis corresponds to the line from ear to ear and alignment in this direction is more precise as the optodes and the surface share the same midline). This leads to an uncertainty between the positions of the optodes and the surface of 7 mm, so this mechanism is likely to be responsible for about half the observed error.

It was noted that some infants allowed their arm to be moved passively while others resisted. Some infants resisted during some repeated stimuli but not others. When the infant resists, the motor cortex would be expected to be activated most strongly, but when the arm is moved passively, the somatosensory cortex may be more active. The neonatal somatosensory cortex lies approximately 10 mm posterior to the motor cortex, introducing a mean uncertainty as to the center of the activation of 5 mm. Furthermore, this paradigm is likely to activate the representations of both the arm and the hand, introducing a further uncertainty. Finally, a further uncertainty arises from estimating the location of the motor cortex (Fig. 4). We estimate that the uncertainty in the position of the motor cortex is likely to be approximately 10 mm.

These potential sources of localization error added in quadrature lead to an overall estimated error of 12 mm, which is more than the mean observed localization error. In future studies, these sources of error could be reduced. For example, we intend to use stereo photogrammetry to provide control points on the helmet and the infant simultaneously, and prior anatomical information can be obtained from MR images.

A frequent criticism of optical images is that the spatial resolution is low. The full width at half maximum of the peak in

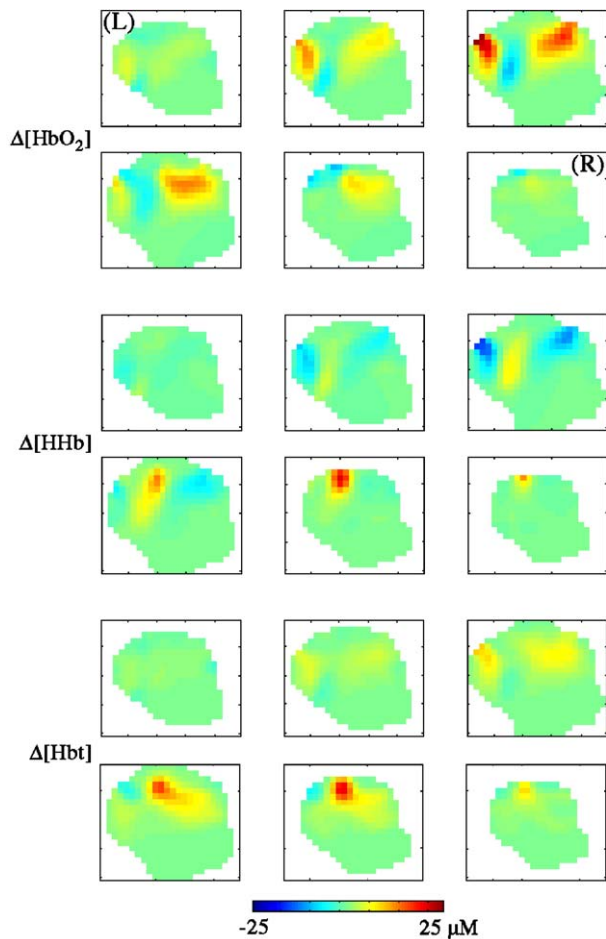


Fig. 5. Images of $\Delta[\text{HbO}_2]$, $\Delta[\text{HHb}]$, and $\Delta[\text{HbT}]$ during left motor activity, showing increases in $\Delta[\text{HHb}]$ and $\Delta[\text{HbT}]$ near the estimated position of the motor cortex. The figure shows 6 sagittal slices from the left (top right) to the right (bottom left) of the head for each of the three parameters.

Fig. 4 is 14.2 mm. This can be improved by reducing λ , but then the quantitative accuracy of the peak change is reduced. The equivalent spatial resolution quoted for fMRI is typically 3 mm, although spatial resolution as low as 1 mm has been reported (Turner and Jones, 2003). However, the fMRI image is typically smoothed with a Gaussian filter of width 7–10 mm prior to statistical analysis, so the equivalent spatial resolution is comparable in the two techniques. Furthermore, clinicians may be reluctant to carry out fMRI on very sick or unsedated babies, whereas optical imaging is carried out at the cot-side.

Functional images

The images obtained demonstrated a predominant increase in $[\text{HbT}]$, as a result of increases in both $[\text{HHb}]$ and $[\text{HbO}_2]$. The amplitude of the measured increase in $[\text{HbT}]$ was $25 \mu\text{M}$ which is greater than the equivalent change observed in near infrared spectroscopy (NIRS) and optical topography. In NIRS, the change is typically of the order of $1 \mu\text{M}$ (Meek et al., 1998, Boas et al., 2001c, Meek, 2002), but this change is averaged over a significant volume of tissue, most of which is not activated, and so NIRS would be expected to significantly underestimate the local change in $[\text{HbT}]$. Optical topography typically reports a somewhat larger

change in $[\text{HbT}]$, of the order of $10 \mu\text{M}$ (Boas et al., 2001c, Taga et al., 2003, Kusaka et al., 2004) due to the improved spatial resolution and hence reduced partial volume effect. The change of $25 \mu\text{M}$ observed here broadly agrees with these quoted values due to the further enhanced spatial resolution of true 3D volume imaging. However, despite appearing physiologically reasonable, these values should be treated with caution as the absolute reconstructed change is dependent on the parameters chosen in the image reconstruction, particularly the regularization parameter λ . If λ is decreased from 0.1 (as used in this work) to 0.01 (equivalent to 1% error in the data and model), the absolute change in $[\text{HbT}]$ increases from $25 \mu\text{M}$ to 1 mM, which is no longer physiologically reasonable. Reassuringly, however, the images remain qualitatively similar. In particular, the localization accuracy and the relative contributions of $\Delta[\text{HbT}]$, $\Delta[\text{HHb}]$ and $\Delta[\text{HbO}_2]$ remain fixed as λ changes.

Both $[\text{HHb}]$ and $[\text{HbO}_2]$ increased during activation. This is consistent with reports of measurement on neonates using NIRS, e.g., Meek (2002), optical topography, e.g., Kusaka et al. (2004) and BOLD fMRI, e.g., Martin et al. (1999) but is different from the usually observed change in adults in whom $[\text{HHb}]$ decreases. Interestingly, the location of the change in $[\text{HHb}]$ and $[\text{HbO}_2]$ did not always coincide (Fig. 5). This illustrates the potential of optical tomography to distinguish between the spatial extent of changes in $[\text{HHb}]$ and $[\text{HbO}_2]$.

In some subjects, there is evidence of changes in $[\text{HbT}]$ in the region of the ipsilateral region motor cortex. In Fig. 4, for example, regions of both increased and decreased $[\text{HbT}]$ can be observed ipsilaterally. Both phenomena have been reported in the literature during fMRI studies (Kim et al., 1993, Hanakawa et al., 2003, Verstynen et al., 2005). In addition, activity was frequently seen in or around the visual cortex (both Figs. 4 and 5 show some evidence of this). The babies did occasionally wake and open their eyes in response to the arm movement. This was stimulus related but did not occur during all the stimuli, so these changes are difficult to interpret.

Conclusion

We have successfully imaged evoked responses using 3D optical tomography by increasing the effective image acquisition rate by combining data acquired sequentially during repeated stimuli. The activation was localized to within 10.8 mm of the estimated position of the contralateral motor cortex and appeared to be physiologically realistic. The absolute scale of the hemodynamic changes appeared to be realistic, but the rescaling and regularization in the image reconstruction must be optimized before these values can be treated with confidence. However, it should be noted that these images were obtained at the bedside of unsedated, premature infants in the intensive care unit. Furthermore, images of $[\text{HbO}_2]$ and $[\text{HHb}]$ were obtained independently of each other, potentially allowing the increased oxygen extraction due to brain activation to be distinguished from the increased blood volume due to vasodilation.

Improvements to the instrumentation which will provide faster data acquisition and a more portable imaging system are underway (Becker et al., 2005). These improvements will allow image acquisition times of the order of 1 s per source to be acquired routinely, improving the ability to record fast events, particularly when combined with sophisticated image reconstruction techni-

ques such as the Kalman filter (Prince et al., 2003, Kohlemainen et al., 2003). Optical tomography will then provide a unique opportunity for recording deep evoked responses at the cot-side. Potential applications include the assessment of function as an early indicator of long-term outcome, the detection of auditory evoked responses as a technique for monitoring depth of anaesthesia (de Cosmo et al., 2004) and the investigation of deep brain function such as the development of pain processing in the newborn (Fitzgerald and Beggs, 2001).

Acknowledgments

We would like to thank Roza Yusof and Gilberto Branco for their assistance with the data acquisition. Support for this work has been generously provided by the EPSRC. AG is funded by an EPSRC Advanced Research Fellowship.

References

- Arridge, S.R., 1999. Optical tomography in medical imaging. *Inverse Probl.* 15, R41–R93.
- Arridge, S.R., Schweiger, M., 1995. Photon measurement density functions: Part II. Finite element method calculations. *Appl. Opt.* 34, 8026–8037.
- Arridge, S.R., Hebden, J.C., Schweiger, M., Schmidt, F.E.W., Fry, M.E., Hillman, E.M.C., Dehghani, H., Delpy, D.T., 2000. A method for 3D time-resolved optical tomography. *Int. J. Imaging Syst. Technol.* 11, 2–11.
- Becker, W., Bergmann, A., Gibson, A., Everdell, N., Jennions, D., Schweiger, M., Arridge, S.R., Hebden, J.C., 2005. Multi-dimensional time-correlated single photon counting applied to diffuse optical tomography. *Proc. SPIE*, 5693.
- Bluestone, A.Y., Abdoulev, G., Schmitz, C.H., Barbour, R.L., Hielscher, A.H., 2001. Three-dimensional optical tomography of hemodynamics in the human head. *Opt. Express* 9 (6), 272–286.
- Boas, D.A., Brooks, D.H., Miller, E.L., DiMarzio, C.A., Kilmer, M., Gaudette, R.J., Zhang, Q., 2001a. Imaging the body with diffuse optical tomography. *IEEE Signal Process. Mag.* 18 (6), 57–75.
- Boas, D.A., Gaudette, T., Arridge, S.R., 2001b. Simultaneous imaging and optode calibration with diffuse optical tomography. *Opt. Express* 8 (5), 263–270.
- Boas, D.A., Gaudette, T., Strangman, G., Cheng, X., Marota, J.J., Mandeville, J.B., 2001. The accuracy of near infrared spectroscopy and imaging during focal changes in cerebral hemodynamics. *NeuroImage* 13 (1), 76–90.
- de Cosmo, G., Aceto, P., Congedo, E., 2004. Auditory evoked responses. *Minerva Anesthesiol.* 70 (5), 293–297.
- Fitzgerald, M., Beggs, S., 2001. The neurobiology of pain: developmental aspects. *Neuroscientist* 7 (3), 246–257.
- Gibson, A.P., Riley, J., Schweiger, M., Hebden, J.C., Arridge, S.R., Delpy, D.T., 2003a. A method for generating patient-specific finite element meshes for head modelling. *Phys. Med. Biol.* 48, 481–495.
- Gibson, A.P., Yusof, R.M., Dehghani, H., Riley, J., Everdell, N., Richards, R., Hebden, J.C., Schweiger, M., Arridge, S.R., Delpy, D.T., 2003b. Optical tomography of a realistic neonatal head phantom. *Appl. Opt.* 42 (16), 3109–3116.
- Gibson, A.P., Hebden, J.C., Arridge, S.R., 2005a. Recent advances in diffuse optical imaging. *Phys. Med. Biol.* 50, R1–R43.
- Gibson, A.P., Hebden, J.C., Riley, J., Everdell, N., Schweiger, M., Arridge, S.R., Delpy, D.T., 2005b. Linear and non-linear reconstruction for optical tomography of phantoms with non-scattering regions. *Appl. Opt.* 44 (19), 3925–3936.
- Gluckmann, P.D., Wyatt, J.S., Azzopardi, D., Ballard, R., Edwards, A.D., Ferriero, D.M., Polin, R.A., Robertson, C.M., Thoresen, M., Whitelaw, A., Gunn, A.J., 2005. Selective head cooling with mild systemic hypothermia after neonatal encephalopathy: multicentre randomised trial. *Lancet* 365, 632–640.
- Hanakawa, T., Immisch, I., Toma, K., Dimyan, M.A., van Gelderen, P., Hallett, M., 2003. Functional properties of brain areas associated with motor execution and imagery. *J. Neurophysiol.* 89, 989–1002.
- Hebden, J.C., 2003. Advances in optical imaging of the newborn infant brain. *Psychophysiology* 40, 501–510.
- Hebden, J.C., Gibson, A.P., Yusof, R.M., Everdell, N., Hillman, E.M., Delpy, D.T., Austin, T., Meek, J., Wyatt, J.S., 2002. Three-dimensional optical tomography of the premature infant brain. *Phys. Med. Biol.* 47, 4155–4166.
- Hebden, J.C., Gonzalez, F.M., Gibson, A.P., Hillman, E.M., Yusof, R.M., Everdell, N., Delpy, D.T., Zaccanti, G., Martelli, F., 2003. Assessment of an in situ temporal calibration method for time-resolved optical tomography. *J. Biomed. Opt.* 8 (1), 87–92.
- Hebden, J.C., Gibson, A.P., Austin, T., Yusof, R.M., Everdell, N., Delpy, D.T., Arridge, S.R., Meek, J.H., Wyatt, J.S., 2004. Imaging changes in blood volume and oxygenation in the newborn infant brain using three-dimensional optical tomography. *Phys. Med. Biol.* 49 (7), 1117–1130.
- Hillman, E.M.C., Hebden, J.C., Schmidt, F.E.W., Arridge, S.R., Schweiger, M., Dehghani, H., Delpy, D.T., 2000. Calibration techniques and datatype extraction for time-resolved optical tomography. *Rev. Sci. Instrum.* 71 (9), 3415–3427.
- Hintz, S.R., Cheong, W.F., van Houten, J.P., Stevenson, D.K., Benaron, D.A., 1999. Bedside imaging of intracranial hemorrhage in the neonate using light: Comparison with ultrasound, computed tomography, and magnetic resonance imaging. *Pediatr. Res.* 45 (1), 54–59.
- Hueber, D., Franceschini, M.A., Ma, H.Y., Zhang, Q., Ballesters, J.R., Fantini, S., Wallace, D., Ntziachristos, V., Chance, B., 2001. Non-invasive and quantitative near-infrared haemoglobin spectrometry in the piglet brain during hypoxic stress, using a frequency-domain multi-distance instrument. *Phys. Med. Biol.* 46, 41–62.
- Kim, S.-G., Ashe, J., Georgopoulos, A.P., Merkle, H., Ellermann, J.M., Menon, R.S., Ogawa, S., Ugurbil, K., 1993. Functional imaging of human motor cortex at high magnetic field. *J. Neurophysiol.* 69 (1), 297–302.
- Kohlemainen, V., Prince, S., Arridge, S.R., Kaipio, J.P., 2003. State-estimation approach to the nonstationary optical tomography problem. *J. Opt. Soc. Am. A* 20 (5), 876–889.
- Koizumi, H., Yamamoto, T., Maki, A., Yamashita, Y., Sato, H., Kawaguchi, H., Ichikawa, N., 2003. Optical topography: practical problems and new applications. *Appl. Opt.* 42 (16), 3054–3062.
- Kusaka, T., Kawada, K., Okubo, K., Nagano, K., Namba, M., Okada, H., Imai, T., Isobe, K., Itoh, S., 2004. Noninvasive optical imaging in the visual cortex in young infants. *Hum. Brain Mapp.* 22, 122–132.
- Martin, E., Joeri, P., Loenneker, T., Ekatothramis, D., Vitacco, D., Ennig, J., Marcar, V.L., 1999. Visual processing in infants and children studied using functional MRI. *Pediatr. Res.* 46, 135–140.
- Meek, J., 2002. Basic principles of optical imaging and application to the study of infant development. *Dev. Sci.* 5 (3), 371–380.
- Meek, J., Firbank, M., Elwell, C.E., Atkinson, J., Braddick, O., Wyatt, J.S., 1998. Regional haemodynamic responses to visual stimulation in awake infants. *Pediatr. Res.* 42, 840–843.
- Prince, S., Kohlemainen, V., Kaipio, J.P., Franceschini, M.A., Boas, D.A., Arridge, S.R., 2003. Time-series estimation of biological factors in optical diffusion tomography. *Phys. Med. Biol.* 48, 1491–1504.
- Schmidt, F.E.W., Fry, M.E., Hillman, E.M.C., Hebden, J.C., Delpy, D.T., 2000. A 32-channel time-resolved instrument for medical optical tomography. *Rev. Sci. Instrum.* 71 (1), 256–265.
- Schöberl, J., 1997. NETGEN—An advancing front 2D/3D-mesh generator based on abstract rules. *Comput. Vis. Sci.* 1, 41–52.
- Schweiger, M., Gibson, A.P., Arridge, S.R., 2003. Computational aspects of diffuse optical tomography. *IEEE Comp. Sci. Eng.*, 33–41 (Nov/Dec).
- Strangman, G., Boas, D.A., Sutton, J.P., 2002. Non-invasive neuroimaging using near-infrared light. *Biol. Psychiatry* 52, 679–693.

- Taga, G., Asakawa, K., Maki, A., Konishi, Y., Koizumi, H., 2003. Brain imaging in awake infants by near-infrared optical topography. *Proc. Nat. Acad. Sci.* 100 (19), 10722–10727.
- Tsujimoto, S., Yamamoto, T., Kawaguchi, H., Koizumi, H., Sawaguchi, T., 2004. Prefrontal cortical activation associated with working memory in adults and preschool children: an event-related optical topography study. *Cereb. Cortex* 14 (7), 703–712.
- Turner, R., Jones, T., 2003. Techniques for imaging neuroscience. *Br. Med. Bull.* 65, 3–20.
- Verstynen, T., Diedrichsen, J., Albert, N., Aparicio, P., Ivry, R.B., 2005. Ipsilateral motor cortex activity during unimanual hand movements relates to task complexity. *J. Neurophysiol.* 93, 1209–1222.
- Volpe, J.J., 2001. Neurobiology of periventricular leukomalacia in the premature infant. *Pediatr. Res.* 50 (5), 553–562.